Chapter 4

STRUCTURAL ANALYSIS OF $Ho_2Ge_2O_7$ AND EFFECT OF NEGATIVE CHEMICAL PRESSURE UPON ITS MAGNETIC PROPERTIES.

4.1 Introduction

The ground states of magnetically frustrated systems (transition metal oxides) are essentially understood by considering two energy scales. The on-site Coulomb repulsion- Hubbard U and the spin-orbit coupling λ [88]. Both of these parameters largely depend upon the topology of ligands. Hence first it is essential to establish a proper structural analysis of a system, since the arrangement of ligands in such systems imparts a strong crystal field effect upon the rare-earth (RE) ion. The ground spin-state is decided by the low-temperature magnetic interaction between two magnetic RE ions which is described through the Dipolar Spin-Ice Model (DSIM) as discussed in chapter 1. It involves the complexity of low-temperature ferromagnetic (FM) dipolar (D_{nn}) and antiferromagnetic (AFM) exchange interaction (J_{nn}). The effect of these magnetic interactions is generally visible at a temperature (T) ≈ 2 K which leads to RE ion-dependent nontrivial magnetic ground states.

Pyrogermanates, having an entirely different crystallographic structure than the titanates, also belong to the class of frustrated system, but its place in spin-ice family is yet a matter of investigation. This is because the magnetic ground state for $Ho_2Ge_2O_7$ resembles that of the spiral arrangement of spins rather than ice-like spin arrangement for conventional cubic

pyrochlores, though both exhibits similar spin relaxation feature as seen in ac-susceptibility response, discussed in chapter 1 [62].

The exact Curie-Weiss temperature as well as the magnetic ground state is yet unknown in $Ho_2Ge_2O_7$ as could be seen from **Table 4.1** given below.

Table 4.1 Curie-Weiss temperature, magnetic ground state, lattice parameter and anisotropy exhibited in few $A_2B_2O_7$. [59]

A(B) ($A_2B_2O_7$)	θ_C or θ_N	Anisotropy	Ground State	a(Å)
Pr(Pb)	?	Easy axis	Quantum spin ice?	10.8721(9)
Nd(Pb)	0.41 K	Easy axis?	Antiferromagnet?	10.8336(4)
Gd(Pb)	0.8 K	Isotropic	Ferromagnet?	10.7292(8)
Tb(Ge)	?	Easy axis	Spin liquid	9.9617(1)
Dy(Ge)	?	Easy axis	Spin ice	9.9290(5)
Ho(Ge)	?	Easy axis	Spin ice	9.9026(6)
Er(Ge)	1.41 K	Easy plane	Antiferromagnet?	9.8767(3)
Yb(Ge)	0.61 K	Easy plane	Antiferromagnet?	9.8306(6)

Making an appreciable enhancement in the pyrochlore lattice parameter by replacing Ge^{4+} with Ti^{4+} in $Ho_2Ge_2O_7$ matrix at B site (ionic radii of $Ge^{4+} < Ti^{4+}$), it is possible to tune J_{nn} since it is more sensitive to change in the lattice parameter as well as the distance between the rare earth spins. Induction of this negative chemical pressure effect in this magnetically frustrated system facilitates to study the nature of ground state spin dynamics through M-T, M-H, and ac-susceptibility measurements. This chapter presents a comprehensive structural analysis of powdered $Ho_2Ge_2O_7$ along with the magnetic response. Consequential efforts were made to consolidate and compare pyrochlore's structural and magnetic properties with pyrogermanates.

4.2 Structural analysis

The crystal structure of $Ho_2Ge_2O_7$ follows tetragonal non-centrosymmetric $P4_12_12$ space group symmetry. The Wyckoff positions for the $P4_12_12$ tetragonal space group, as obtained from the International Tables for Crystallography (2006). Vol. A Space group 92, pp. 368–369. is mentioned in **Table 4.2** [89].

Table 4.2 Wyckoff positions of space group = $P4_12_12$. [89]

Multiplicity	Wyckoff letter	Site symmetry	Coordinates
8	b	1	(x,y,z) (-x,-y,z+1/2) (-y+1/2,x+1/2,z+1/4) (y+1/2,-x+1/2,z+3/4) (-x+1/2,y+1/2,-z+1/4) (x+1/2,-y+1/2,-z+3/4) (y,x,-z) (-y,-x,-z+1/2)
4	a	2	(x,x,0) (-x,-x,1/2) (-x+1/2,x+1/2,1/4) (x+1/2,-x+1/2,3/4)

4.2.1 Rietveld refinement of obtained HRXRD pattern of $Ho_2Ge_2O_7$

There are four independent sites of oxygen atoms for this particular space group, three of whose does not restrict *x, y,* and *z* positions. The fourth oxygen at 4a Wyckoff site poses restriction in coordinates with $x=y$ and $z=0$. Using these designated Wyckoff positions for the tetragonal system as listed in **Table 4.2** Rietveld refinement of the obtained HRXRD pattern of $Ho_2Ge_2O_7$ was obtained. **Figure 4.1** presents the room temperature HRXRD pattern of powdered $Ho_2Ge_2O_7$, with no extra reflections indicating the absence of any impurity phases. We established a satisfactory agreement between the calculated and observed data with the value of R_{wp}=15.7, R_e= 8.26, R_p=12.7, and χ^2 = 3.62. The results of the structural investigations (unit cell parameters and Wyckoff positions) of $Ho_2Ge_2O_7$ are summarized in

Table 4.3. The lattice constants obtained are a = b = 6.8066(5) Å; c = 12.3803(1) Å and unit cell volume V = 573.584 ± 0.008 $Å^3$.

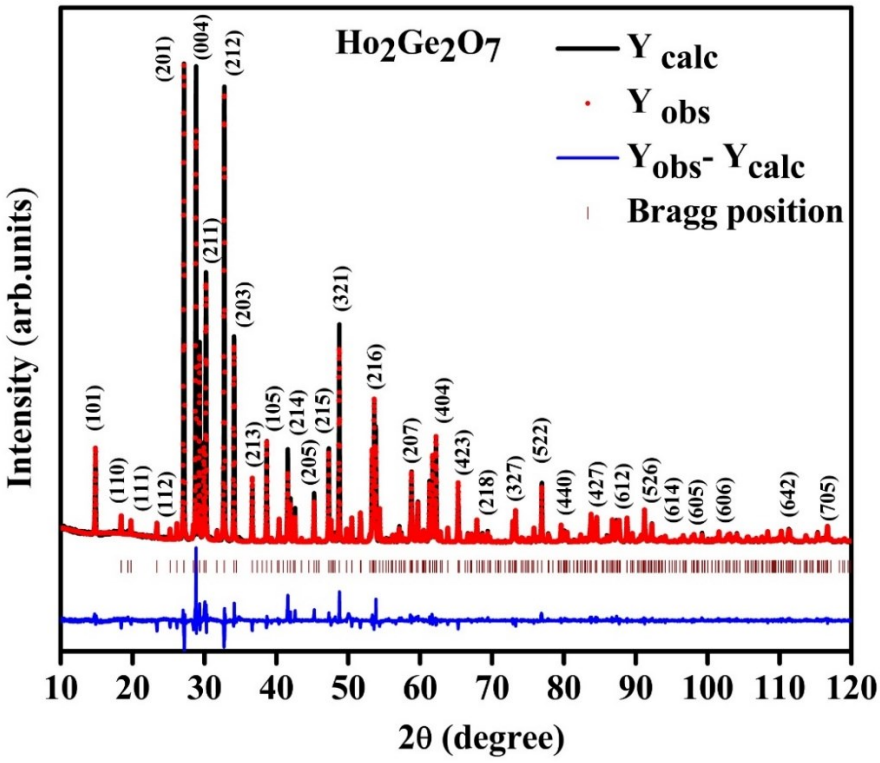

Figure 4.1 Room-temperature high-resolution x-ray diffraction pattern of powdered $Ho_2Ge_2O_7$ along with the fitted [$P4_12_12$(tetragonal) space group] and the difference between the observed and calculated fit.

Table 4.3 Wyckoff positions of $Ho_2Ge_2O_7$ obtained from refinement using space group = $P4_12_12$; Lattice parameters (a = b) = 6.80662(5) Å, c = 12.3803(1) Å; Obtained values of χ^2=3.62, R_{wp}=15.7, R_p= 12.7 and R_e=8.26.

Atomic site	Wyckoff symbol	Atomic coordinates			Thermal parameter B (error)
		x (error)	y (error)	z (error)	
Ho	8b	0.8778(1)	0.3524(1)	0.1351(6)	0.89470
Ge	8b	0.9009(1)	0.1528(2)	0.6194(1)	0.01108
O1	4a	0.301(1)	0.301(1)	0.00000	0.00000
O2	8b	0.0682(8)	0.9668(9)	0.6225(7)	0.62250
O3	8b	0.0582(9)	0.336(1)	0.5790(5)	0.90340
O4	8b	0.6897(9)	0.152(1)	0.5482(4)	0.07088

The basic units of the asymmetric structure of $Ho_2Ge_2O_7$ consist of a pentagonal bipyramidal of Ho^{3+} atom coordinated with seven oxygen atoms, five in *ab* plane, and two obliques to the plane. The network contains a secluded $[Ge_2O_7]^{6-}$ unit in which Ge^{+4} ion is coordinated with four dis-equivalent oxygen atoms forming a tetrahedron with Ge-O_4-Ge unit in common with a bridging angle of 133.3(4) ° as shown in **Figure 4.2**.

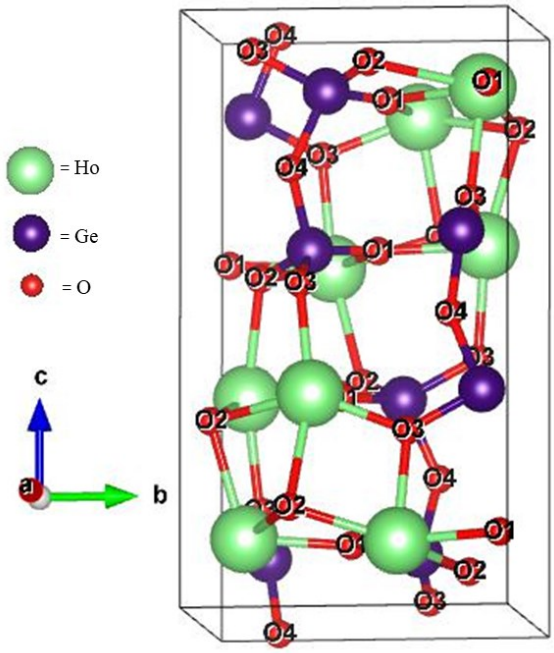

Figure 4.2 3D-structure of $Ho_2Ge_2O_7$ depicting $[Ge_2O_7]^{6-}$ unit in which Ge^{+4} ion is coordinated with four dis-equivalent oxygen with Ge-O4-Ge unit in common having a bridging angle of 133.3(4) °.

This is in good agreement with other lanthanide pyrogermanates, where the Ge-O-Ge angle lies between 130.0° to 136.0°. 3D structure of $Ho_2Ge_2O_7$ as obtained from the Visualization for electronic structural analysis (VESTA), using the structural information, is shown in **Figure 4.3 (a)**. The structure shows the 8 Ho atoms with 2 Ho atoms in each of the four layers

parallel to the crystallographic ab plane. Within a unit cell, the HoO_7 sublattice forms an infinite helical chain of magnetic rare-earth atom parallel to the 4_1 screw axis through the corner-sharing triangle. The pentagonal bipyramidal structure constituting the HoO_7 unit along with GeO_4 tetrahedra could be easily seen in **Figure 4.3 (b)**.

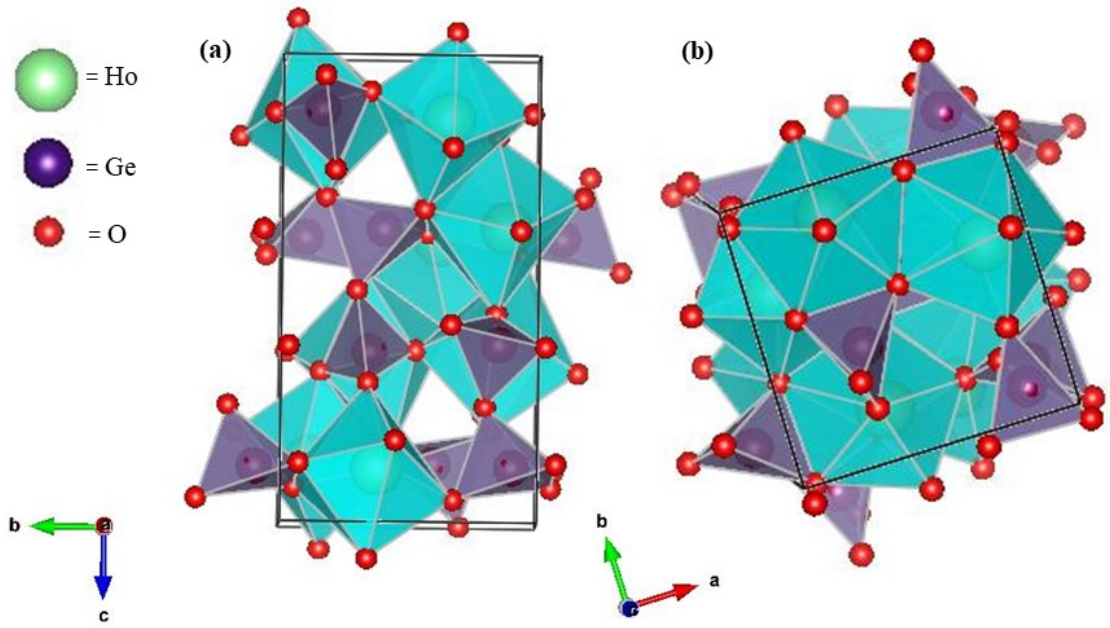

Figure 4.3 Crystal structure of $Ho_2Ge_2O_7$ showing (a) infinite helical chain of magnetic rare-earth atom in a single unit cell having 8 Ho^{3+} atoms with 2 Ho^{3+} atom in each of the four layers parallel to the crystallographic ab plane. (b) The pentagonal bipyramidal structure around the rare-earth ion is constituting the HoO_7 unit along with GeO_4 tetrahedra.

Within a helix, four Ho^{3+} ions are arranged in a pattern of common edge-sharing two triangles further corner joined with next Ho_4 plaquette. This arrangement is shown in the **Figure 4.4**.The average Ho-O bond length turns out to be 2.365 Å, which is linearly and conclusively correlated with increasing ionic radius of the rare-earth ion as the rare earth moves along the lanthanide period. The bond length and bond angle for this structure is listed in **Table 4.4**.

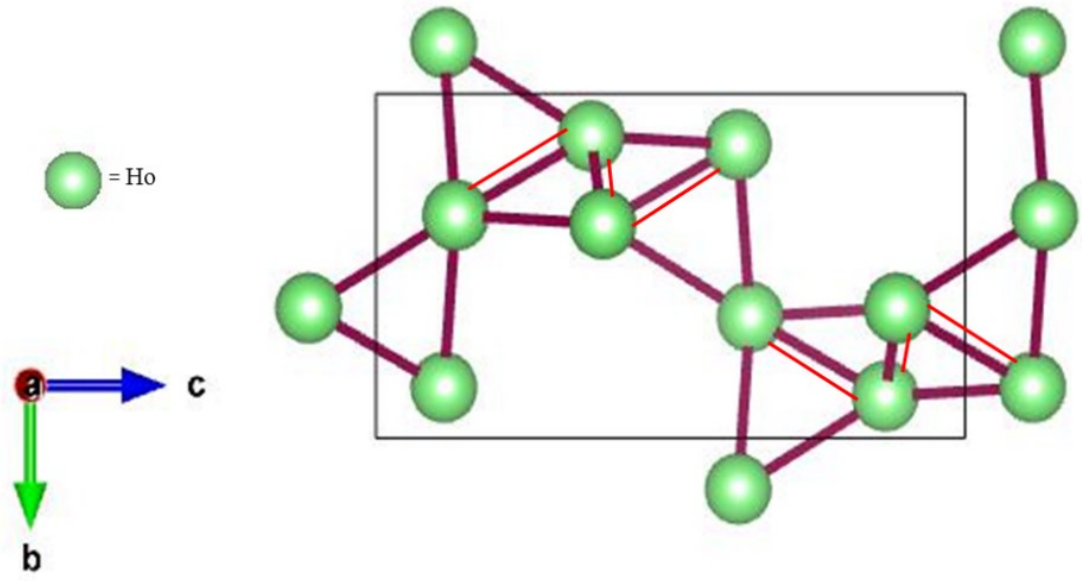

Figure 4.4 Position of magnetic ion within a helix of a unit cell of $Ho_2Ge_2O_7$. It shows four Ho^{3+} ions arranged in a pattern of common edge-sharing two triangles further corner joined with the next Ho_4 plaquette. Shared edges have been marked with a red line.

Table 4.4 Bond length and bond angles as obtained from the 3D structure of $Ho_2Ge_2O_7$ generated from VESTA.

Bond Length (Å)	Bond Angle (°)	Bond Length (Å)	Bond Length (Å)	Bond Angle (°)
Ho-O3 2.494(7)	O4-Ge-O3 112.300(4)	Ge-O1 1.780(4)	O2-O1 2.878(10)	O3-Ho-O4 76.200(3)
Ho-O2 2.209(7)	O3-Ge-O2 97.500(4)	Ge-O2 1.704(7)	O3-O2 2.542(11)	O3-Ho-O3 133.000(3)
Ho-O3 2.565(7)	O2-Ge-O1 111.400(4)	Ge-O3 1.718(8)	O3-O4 2.828(10)	O3-Ho-O4 166.400(3)
Ho-O2 2.442(7)	O1-Ge-O4 98.600(4)	Ge-O4 1.687(7)	O4-O1 2.630(7)	O3-Ho-O2 70.200(3)
Ho-O4 2.297(7)	O1-Ge-O3 112.000(4)		O4-O2 3.014(10)	O3-Ho-O2 89.400(3)
Ho-O3 2.272(8)	O4-Ge-O2 125.500(4)		O1-O3 2.916(2)	(within HoO_7 polyhedron)
Ho-O4 2.278(7)			(within GeO4 tetrahedron)	

4.2.2 Role of negative chemical pressure on the crystal structure of $Ho_2Ge_2O_7$

Followed by the structural analysis of $Ho_2Ge_2O_7$ using the correct space group and coordinates, we have tried to understand the spin dynamics of this particular spin frustrated system by applying negative chemical pressure effect in the $Ho_2Ge_2O_7$**. Figure 4.5** shows the Rietveld refinement of the room temperature HRXRD pattern of $Ho_2Ti_{0.1}Ge_{1.9}O_7$.

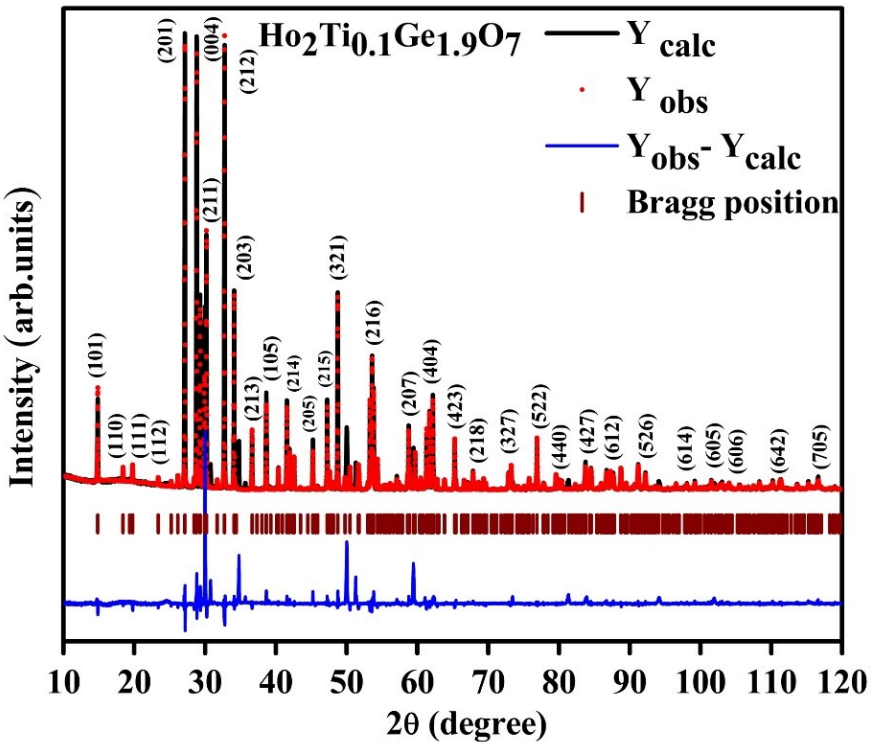

Figure 4.5 Room temperature refined high-resolution x-ray diffraction pattern of powdered $Ho_2Ti_{0.1}Ge_{1.9}O_7$ using the $P4_12_12$ space group.

Wyckoff positions of $Ho_2Ti_{0.1}Ge_{1.9}O_7$ obtained after refinement using space group = $P4_12_12$ are shown in **Table 4.5**. The bong length and bond angles are listed in the **Table 4.6.** Considering the higher ionic radii of Ti^{4+}, its inclusion in the $Ho_2Ge_2O_7$, causes a lattice

volume expansion. The obtained lattice volume for $Ho_2Ge_2O_7$ is 573.584 ± 0.008 $Å^3$, and that for $Ho_2Ti_{0.1}Ge_{1.9}O_7$ is 573.990 ± 0.015 $Å^3$.

Table 4.5 Wyckoff positions of $Ho_2Ti_{0.1}Ge_{1.9}O_7$ obtained after refinement using space group = $P4_12_12$; Lattice parameters (a = b) = 6.8080(1) Å, c = 12.3840(2) Å; Obtained values of χ^2=15.64, R_{wp}=35.2, R_p= 23.9 and R_e=8.91.

Atomic Site	Wyckoff symbol	Atomic coordinates			Thermal parameter B (error)
		x (error)	y (error)	z (error)	
Ho	8b	0.8792(1)	0.3518(4)	0.1350(3)	0.7006(8)
Ge	8b	0.9016(4)	0.1546(2)	0.6187(6)	0.0110(8)
O1	4a	0.2989(7)	0.2989(7)	0.00000	0.0237(4)
O2	8b	0.0600(5)	0.9587(4)	0.6242(4)	0.0091(3)
O3	8b	0.0495(9)	0.3255(6)	0.5810(4)	0.0106(6)
O4	8b	0.6858(4)	0.1520(4)	0.5447(6)	0.0708(8)

Table 4.6 Bond length and bond angles of $Ho_2Ti_{0.1}Ge_{1.9}O_7$ as obtained from using the tools VESTA.

Bond Length (Å)	Bond Angle (°)	Bond Length (Å)	Bond Length (Å)	Bond Angle (°)
Ho-O4 2.2520(14)	O4-Ge-O3 112.6(9)	Ge-O1 1.797(10)	O2-O1 2.88(3)	O3-Ho-O4 86.0(7)
Ho-O2 2.5290(14)	O3-Ge-O2 100.3(8)	Ge-O2 1.715(15)	O3-O2 2.56(3)	O3-Ho-O3 142.0(3)
Ho-O3 2.5440(16)	O2-Ge-O1 110.2(10)	Ge-O3 1.613(18)	O3-O4 2.78(3)	O3-Ho-O4 86.0(7)
Ho-O2 2.1600(14)	O1-Ge-O4 98.7(8)	Ge-O4 1.730(14)	O4-O1 2.67(16)	O3-Ho-O2 77.7(7)
Ho-O3 2.3400(2)	O1-Ge-O3 112.3(9)		O4-O2 3.03(3)	O3-Ho-O2 71.8(5)
Ho-O4 2.2620(14)	O4-Ge-O2 123.1(9)		O1-O3 2.83(3)	(within HoO_7 polyhedron)
Ho-O3 2.582(16)			(within GeO4 tetrahedron)	

The expansion is also confirmed through the shift of (hkl) peaks towards a lower angle with Ti^{4+} substitution, as could be seen from a few of the prominent diffraction peaks shown in **Figure 4.6**.

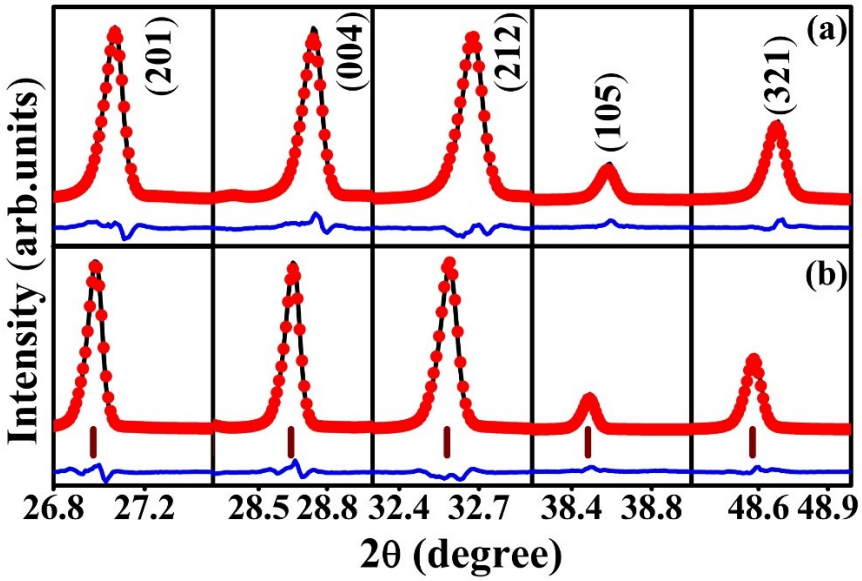

Figure 4.6 Room temperature high-resolution x-ray diffraction pattern for (a) $Ho_2Ge_2O_7$ and (b) $Ho_2Ti_{0.1}Ge_{1.9}O_7$ indicating the shift of (201), (004), (212), (105), and (321) peaks towards lower angle side.

4.3 Magnetic properties of $Ho_2Ge_2O_7$ and $Ho_2Ti_{0.1}Ge_{1.9}O_7$

In this section we will be describing the magnetic properties of $Ho_2Ge_2O_7$ and $Ho_2Ti_{0.1}Ge_{1.9}O_7$ through the temperature dependent magnetization, magnetic field dependent magnetization and temperature dependent ac-susceptibility measurements. These will be subsequently discussed in section in 4.3.1, 4.3.2 and 4.3.3, respectively.

4.3.1 Temperature dependent magnetization.

Figure 4.7 (a) & **Figure 4.7 (b)** present the dc-susceptibility (M-T) of both $Ho_2Ge_2O_7$ and $Ho_2Ti_{0.1}Ge_{1.9}O_7$ at an applied field of 100 & 1000 Oe, respectively. The sample was cooled till 2 K, and zero-field cooled (ZFC) data were collected in the range of 2-200 K under the application of the magnetic field (H= 100 & 1000 Oe) during the warming sequence. Field cooled (FC) data is also collected in the presence of that very same field and recording the data in warming sequence.

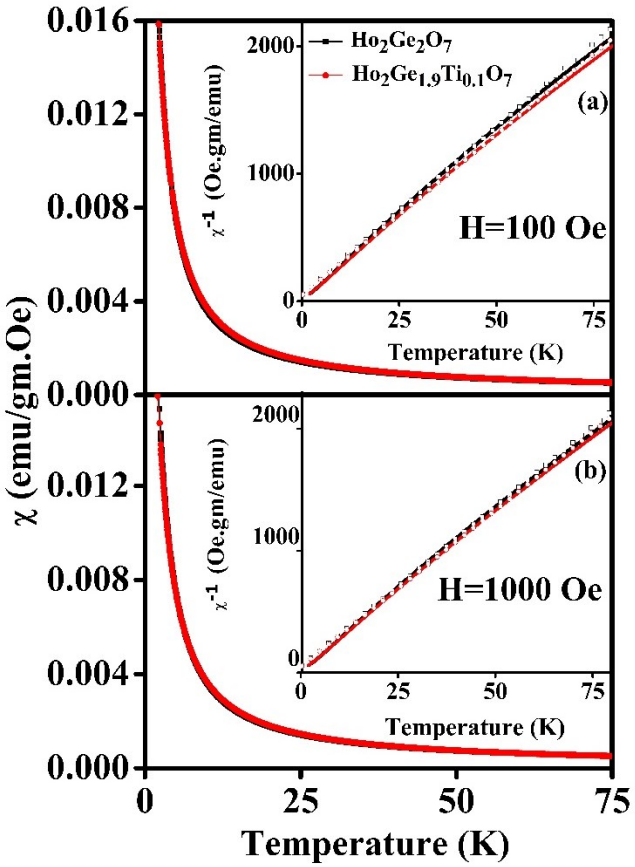

Figure 4.7 Temperature dependence of dc-susceptibility curve of $Ho_2Ge_2O_7$ and $Ho_2Ti_{0.1}Ge_{1.9}O_7$ in the range of (2-200) K for (a) H = 100 Oe & (b) H = 1000 Oe. Inset contains the corresponding inverse susceptibility curve to obtain θ_{CW} fitted through Curie-Weiss law in the linear temperature range of (25-50) K with further extrapolating the χ^{-1} vs. T plot.

A gradual increase in magnetization without any abrupt characteristic implies no evidence of any magnetic phase transition down to the 2 K, which indicates a slow spin alignment process with decreasing temperature. FC and ZFC dc-susceptibility data entirely overlap which excludes the possibility of the formation of a spin-glass state at a lower temperature [45]. This response gives the clear inference of partially ordered, ordered, or ice like ground state, indicating that holmium germanates behave as a soft magnetic material at a lower temperature. Inverse susceptibility curve as shown in the inset of **Figure 4.7 (a)** & **Figure 4.7 (b)** shows a linear response against temperature above 70 K extending till 200 K. Below 70 K; χ^{-1} shows deviation from ideal Curie-Weiss law might be due to the formation of short-range magnetic correlations due to the increase in spin flipping time at lower temperatures. However, no interactions between spins are established until 2 K, which could lead to long-range ordering. Identical behavior is manifested in $Tb_2Ti_2O_7$ and $Tb_2Ge_2O_7$ systems, where the compound is in a typical paramagnetic state with the appearance of short-range spin correlations at a lower temperature [19].

Inverse susceptibility vs. temperature plot has been fitted using equation 3.1 to obtain the Curie-Weiss temperature [90]. In the similar fashion, three different range of temperature, (20-45), (25-50), and (30-55) K, has been used. For the fitting temperature range (20-45) K, θcw increases from -1.44 K to -1.28 K for H = 100 Oe, and from -1.35 K to -1.32 K for H = 1000 Oe. For the temperature range of (25-50) K, θcw increases from -2.04 K to -1.84 K for H = 100 Oe, and from -1.95 K to -1.84 K for H = 1000 Oe. Similarly, for temperature range (30-55), θcw increases from -2.77 K to -2.64 K (H = 100 Oe) and from -2.85 K to -2.50 K (H = 1000 Oe). The values are summarized in **Table 4.7**. Similar trend in θcw was obtained with increase in negative chemical pressure i.e., for sample having composition of

$Ho_2Ti_{0.1}Ge_{1.9}O_7$. The fitting range of (25-50) K has been used for further discussion. The value of θ_{cw} is -2.04 K for $Ho_2Ge_2O_7$. θ_{cw} moves towards a lesser negative value of -1.89 K for $Ho_2Ti_{0.1}Ge_{1.9}O_7$ (H=100 Oe) suggesting a decrement in antiferromagnetic exchange interaction between Ho^{+3} magnetic moments with increase in negative chemical pressure. Saez-Puche *et al.* reported the Curie-Weiss Temperature of powdered tetragonal $Ho_2Ge_2O_7$ to be -4.7 K [91]. The value of obtained Curie-Weiss temperature for H =1000 Oe also evolves, in the same manner, being -1.95 K for $Ho_2Ge_2O_7$ and -1.84 K for $Ho_2Ti_{0.1}Ge_{1.9}O_7$.

Table 4.7 Curie Weiss temperature for $Ho_2Ge_2O_7$ & $Ho_2Ti_{0.1}Ge_{1.9}O_7$ obtained from Curie Weiss fitting at 100 and 1000 Oe. The values in bracket represent the error.

Compound	θ_{cw} (K); H=100 Oe	θ_{cw} (K); H=1000 Oe	θ_{cw} (K); H=100 Oe	θ_{cw} (K); H=1000 Oe	θ_{cw} (K); H=100 Oe	θ_{cw} (K); H=1000 Oe
	Fitting range = (20-45)K		Fitting range = (25-50)K		Fitting range = (30-55)K	
$Ho_2Ge_2O_7$	-1.44(0.48)	-1.35(0.46)	-2.04(0.54)	-1.95(0.54)	-2.77(0.54)	-2.85 (0.63)
$Ho_2Ti_{0.1}Ge_{1.9}O_7$	-1.28(0.44)	-1.32(0.58)	-1.84(0.61)	-1.84(0.58)	-2.64(0.43)	-2.50 (0.74)

4.3.2 Field dependent magnetization

Isothermal magnetization (T=2 K) of $Ho_2Ge_2O_7$ and $Ho_2Ti_{0.1}Ge_{1.9}O_7$ as a function of the magnetic field (0-70 kOe) is shown in **Figure 4.8.** Magnetization increases sharply with field till 5 kOe, which proceeds towards saturation with a very gradual increment till the applied field of 70 kOe. The value of maximum magnetization (M_{max}) of $Ho_2Ge_2O_7$ within the applied field range is 84.14 emu/gm, i.e., 4.3 μ_b/Ho^{3+} ion, indicating ferromagnetic alignment of Ho^{3+} spins at 2 K, and is little less than half the expected value of free Ho^{3+} ion moment (μ_{sat} = 10 μ_B) due to the angular averaging of the powdered sample.

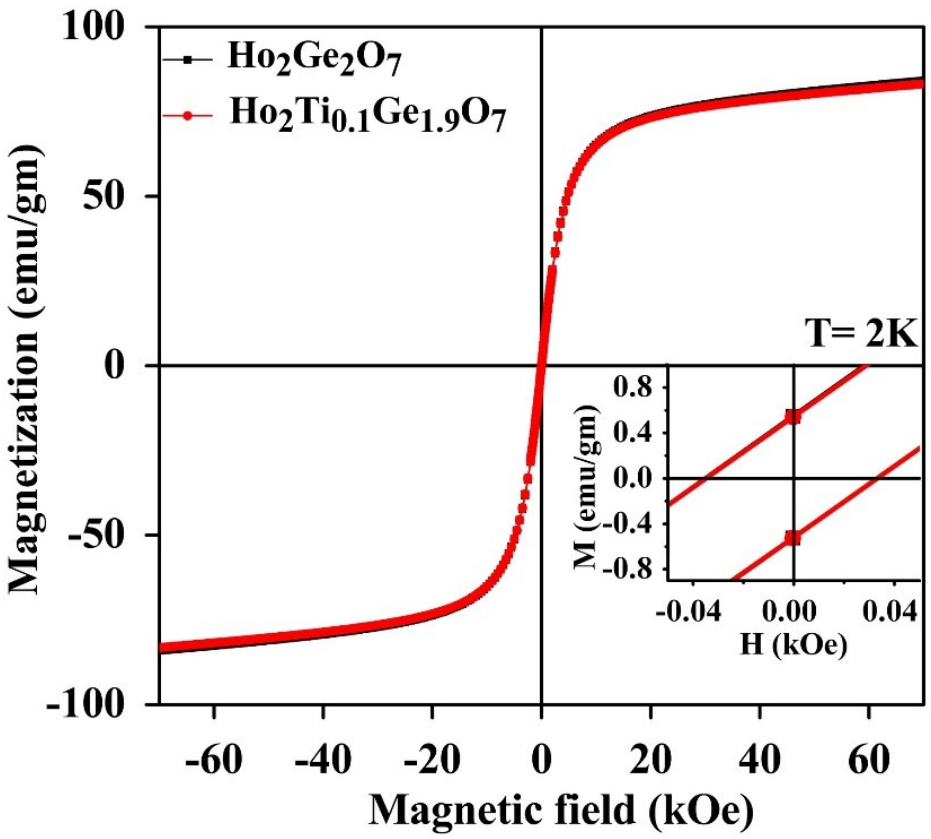

Figure 4.8 Magnetic field dependence isothermal magnetization of $Ho_2Ge_2O_7$ and $Ho_2Ti_{0.1}Ge_{1.9}O_7$ at T = 2 K for H ranging from -70 to 70 kOe.

Interestingly it also follows the similar M-H behavior exhibited for cubic pyrochlore say, $Ho_2Ti_2O_7$ spin ice [27]. The magnetic moment of $Dy_2Ge_2O_7$ (tetragonal) and $Dy_2Ti_2O_7$ (cubic) has already been compared by Ke. X *et al.,* where $Dy_2Ge_2O_7$ has a slightly lower value of saturation magnetization in comparison to $Dy_2Ti_2O_7$ [92]. In $Ho_2Ge_2O_7$ and $Ho_2Ti_{0.1}Ge_{1.9}O_7$, similar behavior could be associated with the strong crystal electric field's anisotropy resulting in a local "Ising behavior" manifested through Ho-Ho coordination in a single Ho_4 plaquette.

Lattice expansion with negative chemical pressure reduces both dipolar (D_{nn}) and exchange interactions (J_{nn}). Even though both interactions decrease, the evolution of θ_{cw} suggests that reduction in exchange interaction dominates over the reduction in dipolar interaction. It could be justified since the dipolar energy D_{nn} is proportional to $1/r_{nn}^3$, and the exchange energy is simply electrostatic interaction varying as $1/r_{nn}$. The separation of the moment (r_{nn}) is of the order of 3.5 Å, which justifies more reduction in J_{nn} in comparison to that of the D_{nn}. T. Sloter *et al.* had established the positive chemical pressure effect in the $Dy_2Ge_{2-x}Si_xO_7$ system where both D_{nn} and J_{nn} increases, but an increase of AFM exchange interaction dominates over that of FM dipolar interaction [21]. Hence, in $Ho_2Ti_{0.1}Ge_{1.9}O_7$, this is possibly accredited to the altered sequence of chemical pressure in an entirely different lattice. It can also be possibly associated with the different electronic ground states (singlet in $Ho_2Ge_2O_7$ and doublet in $Ho_2Ti_2O_7$) due to differences in local crystal field symmetry of Ho^{3+}, which is D_{5h} ($Ho_2Ge_2O_7$) and D_{3d} ($Ho_2Ti_2O_7$).In $Ho_2Ti_2O_7$ and $Dy_2Ti_2O_7$ spin ice, FM dipolar interaction D_{nn} dominates over nearest-neighbor AFM exchange interaction J_{nn} (magnetic ground state); the effective nearest neighbor interaction being given by $J_{eff}S_i^zS_j^z$ where $J_{eff} = m^2(5D_{nn}-J_{nn})/3$ (m=magnetic moment of Ho^{3+}); J_{nn} and D_{nn} being the exchange and dipolar coupling constants; $S_i^z = \sigma_i\vec{z}_i$; $\sigma_i = \pm 1$ and $\vec{z}_i$ are four in equivalent unit vectors pointing from one tetrahedral sublattice to other) [49]. For this J_{eff}, the spins are highly frustrated and end up with a "2 in-2 out" configuration. But for $Ho_2Ge_2O_7$, the obtained value of θ_{cw} (-1.95 K) indicates that there should be long-range AFM ordering in such systems.

4.3.3 Temperature dependent ac-susceptibility

The response of ac-susceptibility with frequency, temperature and applied dc field bias gives better insight of low temperature spin dynamics and how interactions had been tuned in for such a complex spin ice $Ho_2Ge_2O_7$ systems. **Figure 4.9** shows the temperature dependence of the real part of the ac-susceptibility of $Ho_2Ge_2O_7$ down up to 2 K in the absence of dc magnetic field at applied characteristic frequencies of 50, 100, 300, 500, 700, and 900 Hz.

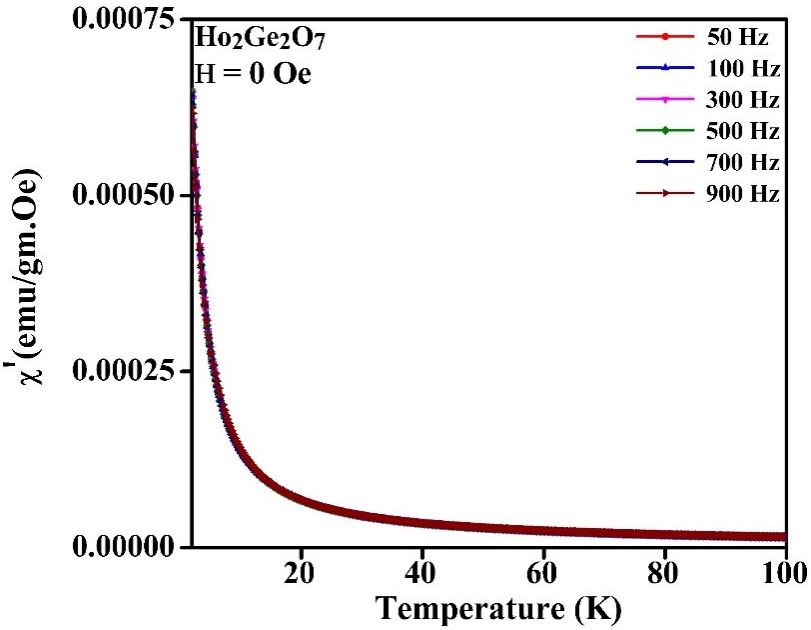

Figure 4.9 Temperature dependence of real part of the ac-susceptibility of $Ho_2Ge_2O_7$ without any application of magnetic field at the characteristic frequency of 50, 100, 300, 500, 700, and 900 Hz.

Without any applied magnetic field, $Ho_2Ge_2O_7$ shows a typical paramagnetic behavior with a monotonous increase in susceptibility having no signature of magnetic ordering down to 2 K. **Figure 4.10** shows ac-susceptibility plot for $Ho_2Ge_2O_7$ and $Ho_2Ti_{0.1}Ge_{1.9}O_7$ under the application of external magnetic field (0.5, 1.0, 5.0, 7.5, 10, 20, and 50 kOe) for an applied frequency of 500 Hz. Contrary to the dc-susceptibility, which rises uniformly with decrease

in temperature followed by the sharp increment below 3 K, ac-susceptibility reveals two spin relaxation features on the application of an external magnetic field. Lower temperature relaxation feature starts appearing at a minimum applied field of 5 kOe centered at 3.2 K, which shifts towards a higher temperature side with an increase in the magnetic field, firmly defying its AFM origin.

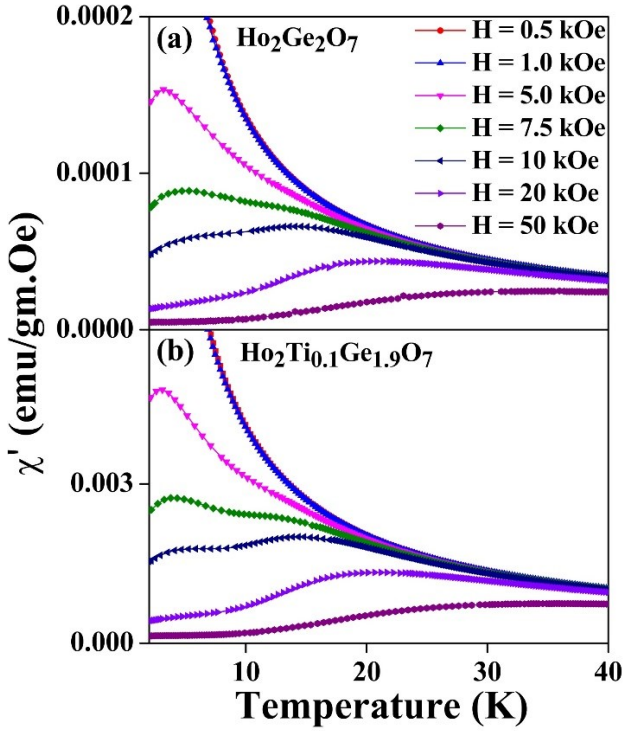

Figure 4.10 Real part of ac-susceptibility of for (a) $Ho_2Ge_2O_7$ and (b) $Ho_2Ti_{0.1}Ge_{1.9}O_7$ as a function of temperature (2-40) K at an applied magnetic field of 0.5, 1.0, 5.0, 7.5, 10, 20 and 50 kOe (applied frequency = 500 Hz).

Had this feature been of AFM origin, an increase in the magnetic field's magnitude would have suppressed it towards the lower temperature side. This shifting with field enhancement suggests it to be of ferromagnetic origin and is most likely associated with the emergence of local short-range spin correlation [19]. Specific heat measurement on single-crystal $Ho_2Ge_2O_7$ had already established the development of short-range correlations above the 3d ordering

temperature, which is of ferromagnetic nature, while long-range ordering reveals significant antiferromagnetic nature [28]**.** Such a field-driven magnetic transition in $Ho_2Ge_2O_7$ can be characterized as a metamagnetic transition (MMT). It results due to the reorientation of the spins at the anisotropic magnetic site in response to the applied field. Similar short-range local ferromagnetic spin correlations are also manifested in $Tb_2Ge_2O_7$, whereas $Dy_2Ge_2O_7$ exhibits long-range antiferromagnetic ordering at 2.3 K [92]. Relative lowering in peak intensity corresponding to this feature is manifested. With an increase in the magnetic field to 7.5 kOe, the second relaxation peak emerges towards the higher temperature side at 14 K (single ion freezing; T_s), which is a characteristic thermally induced peak due to initiation in freezing of single ion spin fluctuations [28]. Both the peaks get almost flattened at an applied field of 50 kOe.

The shift of T_s towards the higher temperature side with an increase in the applied magnetic field is shown in **Figure 4.11**. In $Ho_2Ti_2O_7$, neutron spin-echo (NSE) studies establish thermally driven single ion spin relaxation process for $T > 15$ K, and for $T < 15$ K, spin dynamics is cumbersome, attributed to quantum tunneling between possible spin states [36]. The lower temperature, quantum spin relaxation feature is also manifested in $Dy_2Ti_2O_7$ and $Dy_2Sn_2O_7$. However, in $Ho_2Ge_2O_7$ spin relaxation feature corresponding to $T \approx 3$ K exhibits a shift upon the application of chemical pressure in the $Ho_2Ge_2O_7$. Coming to **Figure 4.10** where ac-susceptibility curve of $Ho_2Ge_2O_7$ has been plotted along with its negative chemical pressure derivative $Ho_2Ti_{0.1}Ge_{1.9}O_7$.

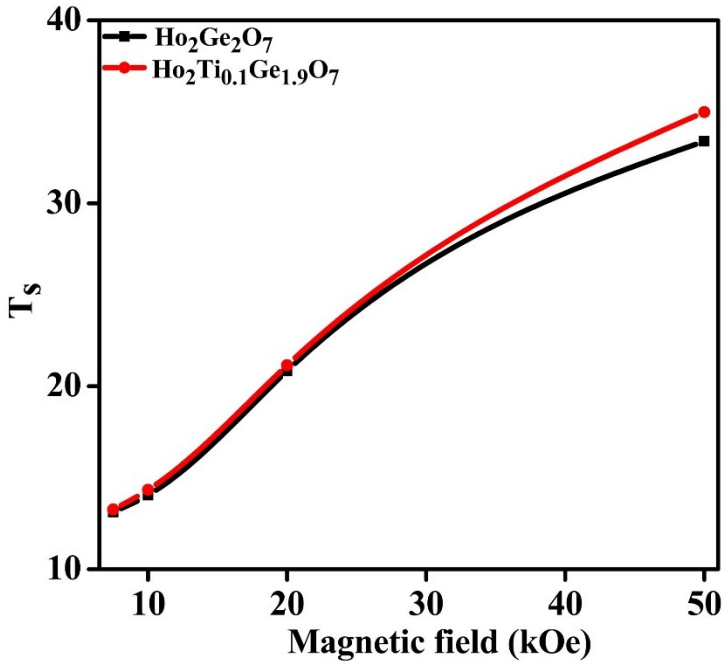

Figure 4.11 The variation in the single ion freezing temperature with a magnetic field for (a) $Ho_2Ge_2O_7$ and (b) $Ho_2Ti_{0.1}Ge_{1.9}O_7$.

With a decrease in chemical pressure, the feature corresponding to ferromagnetic correlations between spins shifts towards lower temperature, as shown in **Figure 4.12.** As discussed earlier, lattice volume expansion can weaken both the dipolar and exchange interaction due to negative chemical pressure. The spin ice system's dipolar interactions are of ferromagnetic origin, and its reduction explains the shift in T_s towards lower temperature with negative chemical pressure. It indicates the absence of quantum spin relaxation phenomenon in $Ho_2Ge_2O_7$ for lower T regime (≈ 3 K) probably due to the difference in crystal field environment associated with different structures compared to the cubic pyrochlore $Ho_2Ti_2O_7$.

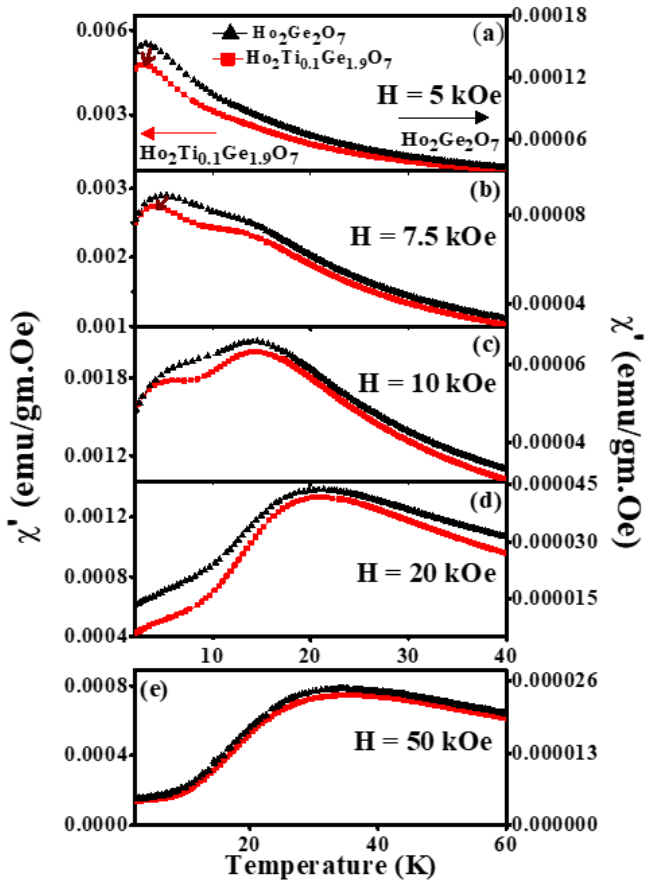

Figure 4.12 The ac-susceptibility plot of $Ho_2Ge_2O_7$ and $Ho_2Ti_{0.1}Ge_{1.9}O_7$at an applied magnetic field of (a) H = 5 kOe (b) H = 7.5 kOe (c) H = 10 kOe (d) H = 20 kOe (e) H = 50 kOe.

$Dy_2Ge_2O_7$ (tetragonal) isostructural to $Ho_2Ge_2O_7$ also marks the absence of quantum spin relaxation since both spin relaxation feature exhibits frequency dependence with temperature [92]. The interplay of dipolar and exchange interactions between Ho^{3+} atoms (across *ab* plane and along *c* axis) in the complex spin structure of $Ho_2Ge_2O_7$ can tune the spin dynamics through chemical pressure. The result demonstrates that spin freezing of $Ho_2Ge_2O_7$ is associated both with thermally activated single ion spin relaxation at 14 K and with collective relaxation of correlated clusters of spins of ferromagnetic origin at 3.2 K.

4.4 Conclusions

Detailed structural analysis of $Ho_2Ge_2O_7$ has been presented using the correct Wyckoff site for the $P4_12_12$ space group. Magnetic response of powdered $Ho_2Ge_2O_7$ (tetragonal) closely resemble that of cubic $Ho_2Ti_2O_7$. In pyrogermanates, the low-temperature short-range spin correlation is of ferromagnetic origin, unlike that of quantum tunneling phenomenon (spin ice configuration) in $Ho_2Ti_2O_7$ which is due to the difference in crystal field potential around the rare-earth ion because of dissimilar oxygen environment. The ac- susceptibility measurements suggest this system to be a classical spin ice material. With the reduction in chemical pressure in the $Ho_2Ge_2O_7$, the decrement of antiferromagnetic exchange interaction (J_{nn}) to be dominant over the decrease in ferromagnetic dipolar interaction (D_{nn}) has been established. It has been shown that these interactions can further be tuned through the structural distortions. Single ion spin freezing around 14 K is prevalent this spin ice materials. After studying the spin relaxation mechanism and magnetic properties of these pyrochlore oxides, we moved on to perform the electronic studies of these systems to look for its possibility in materiality applications. The same is discussed is next chapter.